

Unravelling Water and Salt transport in Polyamide with Nuclear Magnetic Resonance Spectroscopy

Mahsa Abbaszadeh,[†] Ji Il Choi,[‡] Yudan Chen,[¶] Johannes Leisen,[§] Madeline
Garell,[†] Seung Soon Jang,^{*,||} Yan-Yan Hu,^{*,¶,⊥} and Marta C. Hatzell^{*,†,#}

[†]*George W. Woodruff School of Mechanical Engineering*

[‡]*School of Material Science and Engineering, Georgia Institute of Technology, Atlanta*

[¶]*Department of Chemistry and Biochemistry, Florida State University, Tallahassee*

[§]*School of Chemistry and Biochemistry, Georgia Institute of Technology, Atlanta*

^{||}*School of Material Science and Engineering, Georgia Institute of Technology, Atlanta*

[⊥]*Center of Interdisciplinary Magnetic Resonance, National High Magnetic Field*

Laboratory, 1800 East Paul Dirac Drive, Tallahassee, FL 32310, USA.

[#]*School of Chemical and Biomolecular Engineering, Georgia Institute of Technology,
Atlanta, GA, 30332 USA*

E-mail: seungsoon.jang@mse.gatech.edu; yhu@fsu.edu; marta.hatzell@me.gatech.edu

Abstract

Unraveling water and salt transport in polyamide is of growing importance as the use of reverse osmosis membranes grows in many industries. Here, using solid-state nuclear magnetic resonance (NMR) spectroscopy, we measure the translational diffusion coefficients using pulsed-field gradient NMR, examine ion dynamics with NMR relaxometry, and determine activation energy barriers of hydrogen and sodium ions in ion-exchanged polyamide using variable-temperature NMR. We identify two predominant diffusion components within the spectra associated with bound and unbound hydrogen and sodium ions. We show that the diffusion coefficient of the bound hydrogen ions decreases by 46% while the free hydrogen diffusion coefficient remained constant as the salinity of the mixture increases from 1 M to 2 M. Conversely, the diffusion coefficient of bounded sodium did not change while the unbounded sodium diffusion coefficient decreased by 38% as the salinity of the mixture increases from 1 M to 2 M. Through examining the spin-lattice relaxation time (T_1) at various temperatures we reveal that the sodium and hydrogen ion motion decreases with an increase in salinity, and we also report the associated activation energy. We believe these molecular-scale measurements can aid in extending the solution-diffusion model of reverse osmosis membranes.

Introduction

The development of highly permeable thin film composite polyamide membranes with high salt rejection has allowed reverse osmosis (RO) to become the leading technology for seawater and industrial water desalination.^{1,2} Commercial RO membranes have an active aromatic polyamide layer which is formed by interfacial polymerization.³⁻⁶ At a macroscale, commercial polyamide RO membranes achieve near ideal salt rejection ($> 98\%$), high water permeability ($2 - 20 \text{ L m}^{-2} \text{ h}^{-1} \text{ bar}^{-1}$), and low salt permeability ($0.1 - 0.4 \text{ L m}^{-2} \text{ h}^{-1}$).⁵⁻⁷ This high salt rejection is largely ascribed to the unique nonporous and highly tortuous nature of the polyamide layer.⁶

Water and salt transport properties through polyamide is largely limited to physics extrapolated from the solution-diffusion model.^{1,8} For instance, bench scale measurement of water and salt permeability is commonly used to extract water and salt diffusion coefficient.^{5,9,10} While the solution-diffusion model is well tested, the model assumes that chemical and hydraulic gradients are constant, and that all transport processes occur under equilibrium conditions.^{9,11} These and other core assumptions of the solution-diffusion model are becoming increasingly limiting as the field moves beyond seawater as the primary feed-streams.¹¹⁻¹⁴

The transition state theory (TST) model is an alternative to the solution-diffusion model which begins to explore microscopic phenomenon associated with water and salt transport. In the TST model, salt and water partitioning and molecular diffusion is considered an activated process. Thus salt and water must contain enough energy to overcome various transition states within the membrane in order to permeate through the membrane.¹⁵ The transition states within the membrane largely depends on molecular-scale interactions between the polymer, water, and ions. In order to improve the TST model, there is a need for experimental verification of water and salt activation energy, and translational and rotational diffusion coefficients. This type of verification is attained through the use of molecular simulations and advanced characterization.¹⁶

Advanced characterization techniques which aim to extrapolate water and salt transport in membranes include transmission electron microscopy (TEM), quasielastic and inelastic neutron scattering (QENS,INS), Extended X-ray absorption fine structure (EXAFS), full-field Transmission X-ray Microscopy 2D and 3D (TXM-CT and microCT), positron annihilation lifetime spectroscopy (PALS), and Nuclear Magnetic Resonance (NMR) spectroscopy.¹⁷⁻²¹ The average water diffusion coefficient was recently obtained generating a 3D mapping of polyamide density from TEM images, and found to be in the range of $1.03 \pm 0.02 - 1.67 \pm 0.04 \times 10^{-9} \text{ m}^2/\text{s}$.¹⁸ The water diffusion was calculated by converting the 3D nanoscale intensity distributions (density and thickness) to nanoscale distributions of den-

sity, from which the water diffusion coefficient was extracted within polyamide films.¹⁸ It was concluded that aromatic polyamide membranes contain water channels.

Quasielastic neutron scattering experiments suggests that the water diffusion coefficient is $1.9 \pm 0.4 \times 10^{-9} \text{ m}^2/\text{s}$.²² While, molecular dynamics simulations of a hydrated polyamide membrane suggest the diffusion coefficient of the bulk phase is ($3.08 \times 10^{-9} \text{ m}^2/\text{s}$), the interface region is ($0.58 \times 10^{-9} \text{ m}^2/\text{s}$), and the polyamide membrane is ($0.24 \times 10^{-9} \text{ m}^2/\text{s}$).²³ A transmission XAFS provides absorption coefficient for thin film samples; however, one drawback is that samples should have very smooth surfaces, which is not found with polyamide. Positron annihilation lifetime spectroscopy (PALS) coupled with modeling study can also assist in deriving diffusion coefficients in membranes.²⁴ Examining sodium diffusion in polyamide is feasible through ^{23}Na NMR.²⁵ NMR is also effective for determining the purity, degree of cross-linking, and chemical composition of polyamide systems using ^{13}C MAS techniques.^{26,27} Examining the polymer chemistry (reaction mechanism, chemistry of polymer and effects of treatment processes) and dynamics of water in other types of polyamide materials with different chemistry (i.e., nylons) is routinely examined with NMR.²⁸⁻³¹

Herein, we examine the use of solid state NMR to extract the diffusion and activation energy barrier for water and salt in polyamide. We have prepared ion-exchanged polyamide membranes where we introduced the polyamide different salt mixtures (ionic strength = 1 and 2M) and different levels of relative humidity (0, 60 and 98%). We applied pulsed field gradient (PFG) NMR experiments to examine the translational diffusion coefficients of hydrogen and sodium ions in ion-exchanged polyamide.^{32,33} We have measured ^1H and ^{23}Na NMR spin-lattice relaxation time (T_1) for ion-exchanged polyamide at varying RH and salinity. Through monitoring the spin lattice relaxation time (T_1) at various temperatures we also extract the activation energy for salt and water transport.

Results & Discussion

Hydrogen and Sodium Diffusion in Fully Hydrated Polyamide

First, we examine the translational (Figure 1-a) and rotational (Figure 1-b) motion of water (^1H) in fully hydrated polyamide as salinity increases from 1M to 2M using pulse field gradient NMR (PFG-NMR). As the salinity doubled, there is a clear broadening of the ^1H line-width spectra (Figure 1-a and Figure S1 and S3) indicating that the rotational movements are hindered in the presence of higher salt concentration. When examining chemically and magnetically inequivalent components within the ^1H spectra, we identified four peaks. Two peaks follow a 2-component distribution model (≈ 5 ppm). The diffusion coefficient attributed to the peak ≈ 1.3 ppm were unchanged under all conditions (changes in applied gradient pulse (Δ) and salinity), and thus were assumed to be ascribed to the polymer functional groups. The second two were ascribed to bound and unbound hydrogen. The two bound and unbound hydrogen diffusion coefficients changed with salinity and were attributed to the ^1H resonance around 5 ppm.

When examining the rotational and translational motion of water within polyamide, as the salinity increases from 1M to 2M, (Figure 1 a - green line) the unbound hydrogen decreases from 14.7% to 4.6% and the amount of bound hydrogen increases from 82.3 % to 94.4% (as determined by deconvolution of line-shapes as shown in Figure S1). When examining the normalized intensity of the ^1H as a function of different gradient strengths we observe a relaxation (Figure 1-b) for water component at ≈ 4.7 ppm. The Stejskal-Tanner equation allows the extraction of diffusion coefficients (Equation 3). The unbounded hydrogen diffusion coefficient (D_1) does not change with salinity (Figure1-b, Table 1). The unbound hydrogen diffusion coefficient is in the range of 4.7×10^{-10} - 4.9×10^{-10} m^2/s which is lower than the bulk water (self) diffusion coefficient ($2.3 \times 10^{-9} \text{m}^2/\text{s}$) (Table 1).³⁴ The values for self-diffusivity of water in polyamide in this work are also lower than the value for self-diffusivity of bulk water (2.5×10^{-9} m^2/s at 300 K) reported by quasi-elastic neutron

scattering.³⁵ Diffusion of unbound hydrogen is not impacted by increases in salinity. This is not surprising as the molar concentration of water (approximately 55M) is significantly higher than either salt.

The diffusion coefficient of the bound protons decreases from $7.4e^{-11}$ to $4.0e^{-11}$ m^2/s with the addition of 1M KCL (Figure1-c, Table 1). The diffusion of bound protons decreases by 46% with the addition of 1M KCl to a 1M NaCl feed stream (Figure 1c and Table 1). This is due to the increase of salt within the polyamide, which sterically blocks the motion of bound protons.³⁶ It should be noted that the self-diffusion coefficient of water at room temperature is reported to be at 2.8×10^{-9} m^2/s .¹ The presence of more than one diffusion coefficient for 1H could be due to strong hindrance of water mobility in the dense polyamide network, as water molecules are diffusing from a local to bulk diffusion pathway. Here, we assume that the bound water is the molecules that are associated by hydrogen bonding to the oxygen-containing functional groups and fill the polyamide voids (Figure 2). The bound water can be transported (translational motions) across the membrane by being combined with the membrane through hydrogen bonding. Bound water migrates by water molecules hopping from one hydrogen site to another. When salt is added the bounded hydrogen-containing molecules are hindered from interactions with water and/or hydroxide functional groups due to the presence of potassium. The tightness of these bound-water regions depends on the presence of additional ions. As salinity increases, the space around the bound water region is tighter leading to a decrease in the bound water diffusion coefficient. The bound hydrogen diffusion behavior in polyamide is dependent upon interactions with dipoles of hydroxyl of polyamide, water-water, water-polymer, water-sodium-potassium, and electrostatic interactions.

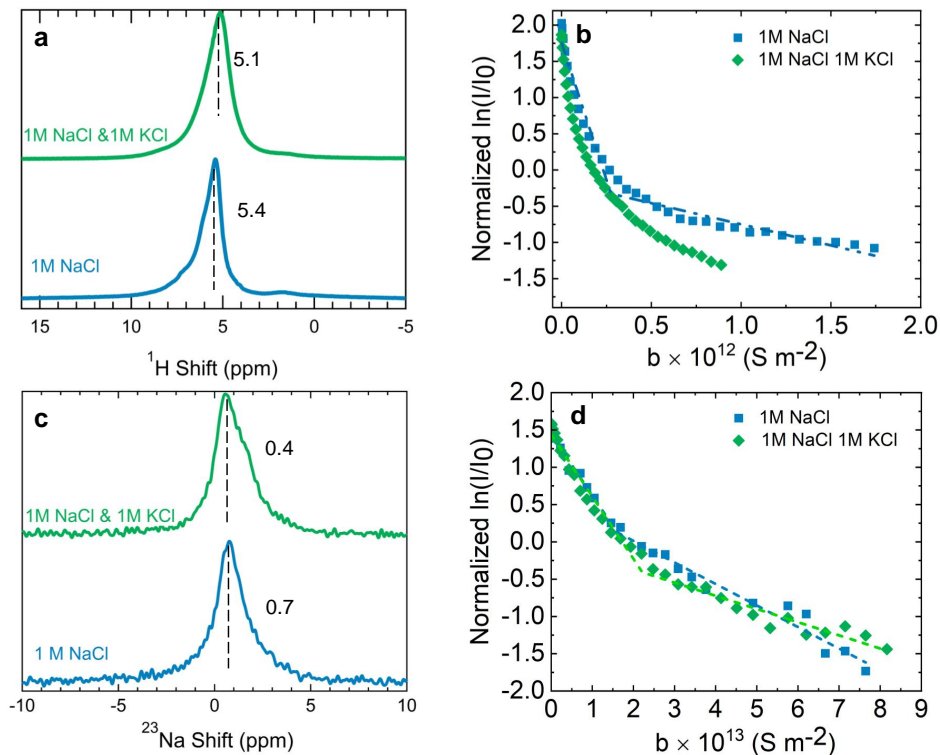


Figure 1: ^1H and ^{23}Na NMR for probing local environments and diffusion coefficients. a) ^1H NMR spectra, b) D_1 and D_2 fitting of ^1H PFG NMR decay for hydrogen translational motion (diffusion), c) ^{23}Na NMR spectra, d) D_1 and D_2 fitting of ^{23}Na PFG NMR decay on sodium translational motion (diffusion).

Next, we examine the translational (See Figure 1-d) and rotational (see Figure 1-c) motion of salt (^{23}Na) in polyamide as salinity increases from 1M to 2M using pulse field gradient NMR (PFG-NMR). As the salinity doubled, like the ^1H spectra, there is also a clear broadening of ^{23}Na line-width spectra (Figure 1-c and Figure S2). This again indicates that the rotational and translational movements are hindered in the presence of higher salt concentration. When examining the number of diffusion components within the ^{23}Na spectra, we identified two peaks. They were ascribed to bound and unbound sodium (Figure 1-c and Figure S2). When examining the rotational and translational motion of sodium within the membrane, as the salinity increases from 1M to 2M, (Figure 1 c - green line) the unbounded sodium decreases from $\sim 87\%$ to $\sim 75\%$ and the amount of bounded ions increases from 12.5 % to 24.6% (as determined by deconvolution of line-shapes as shown

in Figure S2). Thus, the hindrance in sodium ion movement is due to the increase in the amount of sodium that exists in the bounded state in the presence of high salinity.

When examining the normalized intensity of the ^{23}Na as a function of different gradient strengths we observe a relaxation (Figure 1-d). The unbound sodium diffusion decreases by 38% from 9.4 to $5.8 \times 10^{-12} \text{ m}^2/\text{s}$ (Figure 1-d and Table 1). The decrease in the unbound diffusion coefficient of sodium may be due to the competitive diffusion between sodium and potassium as salinity increases. The bounded diffusion coefficient (D_2) does not change as the ionic strength increases, and remains around $0.2 \times 10^{-12} \text{ m}^2/\text{s}$ (Figure 1-d and Table 1). Self-diffusion coefficients of sodium ions in polyamide in this work are also lower (approximately 10 orders of magnitude) compared to self diffusion of sodium in relative concentration of sodium chloride solution.³⁷ This is due to the fact that there are most likely low concentrations of sodium physiochemically interacting with the polymer as sodium is able to freely move within the free space of the polymer. We deduce that with increase in salinity, the translational movements of the unbounded sodium ions passing through polyamide are hindered. For unbounded sodium ions, the high salinity reduces Brownian motion and provides accessible open space for the translation motions of sodium ions. In this case, sodium ions with a large hydrodynamic radius than potassium ions encounter more boundaries and thereby can only travel smaller distances. Our results show that the bound and unbound diffusion coefficients of sodium ions in ion-exchanged polyamide are less than the sodium ion diffusion reported in water ($D_{\text{NaCl}} = 1.6 \times 10^{-9} \text{ m}^2/\text{s}$).³⁸ The ion transport in polymeric membranes is usually governed by Donnan exclusion, dielectric exclusion, and size exclusion. Since the ion-exchanged polyamide membrane contains the same functional groups with similar charge properties in different ionic mixtures, the PFG NMR diffusometry results suggest that a size-exclusion mechanism dominates the ion translational motions resulting from the dense structure of the polyamide network.³⁹

Table 1: Diffusion Coefficient measurements derived from PFG experiment for fully hydrated ion-exchanged polyamide

Diffusion PFG Experiments			
Multi-ionic Mixture	Nuclei	D_1 (unbounded) ($m^2.S^{-1}$)	D_2 (bounded) ($m^2.S^{-1}$)
1M NaCl	^{23}Na	9.4×10^{-12}	0.2×10^{-12}
1M NaCl+ 1M KCl	^{23}Na	5.8×10^{-12}	0.2×10^{-12}
1M NaCl	1H	4.9×10^{-10}	7.4×10^{-11}
1M NaCl+ 1M KCl	1H	4.7×10^{-10}	4.0×10^{-11}

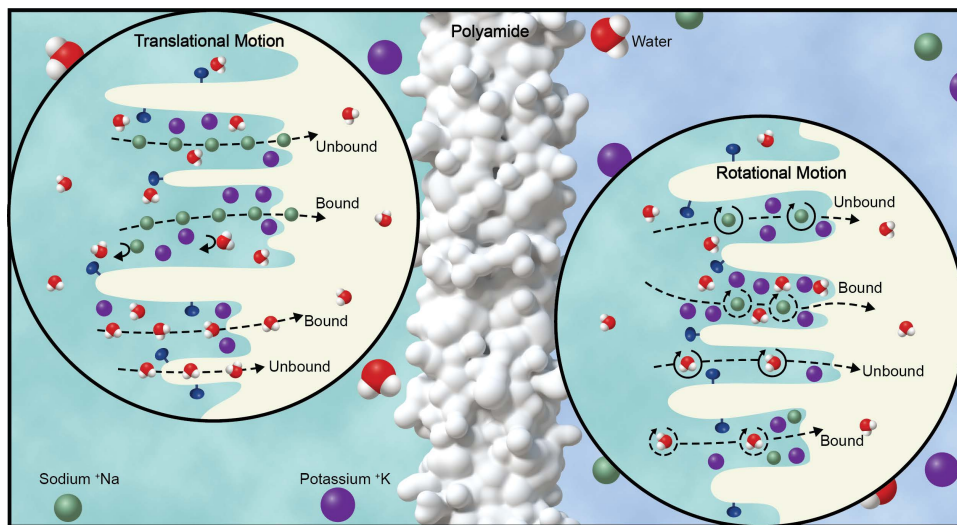


Figure 2: Schematic of ionic translational and rotational motions in polyamide. The motion of Relatively mobile "unbounded/free" water/sodium and relatively immobile "bounded" water/sodium.

Ion Dynamics at Polyamide Interface by Magic-Angle Spinning Solid-State NMR

Herein, we used magic angle spinning (MAS) to produce high-resolution NMR spectra to characterize the ion dynamics in polyamide. MAS NMR spins the sample at the magic angle (54.74°) with respect to the direction of the magnetic field. This allows us to have high-resolution data where the effects of dipolar, chemical shift anisotropy, and quadrupolar interactions are ruled out. MAS is a powerful method for analyzing chemical environments

in an atomic level.

The peak positions (chemical shifts) of the and the line width of the ^1H signal vary with changes in relative humidity and salinity (Figure 3 a). At low relative humidity ($\text{RH} \sim 0\%$), the physics examined is mainly due to the properties of the polymer. Ideally, enhanced transport within the polymer itself can allow enhanced transport within the hydrated polymer, which is important to examine. Without hydration, the ($\text{H}_2\text{O}/\text{OH}^-$) motion is ascribed to hindered movements within the pores, at the membrane interface and outside the pores (Figure 3-a). At low relative humidity, when salinity increases, the ^1H peak positions shift toward lower values (ppm) slightly. As the ^1H shifts upfield (lower ppm values), we hypothesized the peaks of hydrogen are attributed to water (hydrogen) bonding with amine functional groups. Reversely, as the ^1H peak shifts downfield (higher ppm values), we hypothesize that water molecules (hydrogen) bond with carboxylic acid functional groups of polyamide.⁴⁰ We assume as the polyamide is more decorated with linear chains on the interface (carboxylic acid functional groups) and more fully crosslinked aggregates (amide functional groups) in the core part of polymer,⁴¹ a lower ppm value in ^1H demonstrates the interaction of hydrogen ions with amide-containing functional groups which implies a in the pore behavior for the ion .

At high relative humidity ($\text{RH} \sim 98\%$), the physics examined is largely due to polymer-water interactions. With hydration, we observed a sharp peak in the ^1H spectra, indicating fast rotational motions of water molecules. Increased molecular mobility is expected because water hydrates the polymer. This phenomenon results in an increased effective magnetic field (higher ppm values) and this effect can be caused by the presence of specific functional groups that withdraw electron density from hydrogen ions, such as amide functional groups in polyamide. This gives us information that the hydrogen ions are closer to amide functional groups as the relative humidity of the membranes increases. However, with high relative humidity, when salinity increases, the ^1H spectra shift upfield by 2.4 ppm (Figure 3-a). Furthermore, the signal that indicates that water within the pores vanishes. Therefore, as

salt infiltrates the pores, water is displaced to the polyamide interface (Figure S1).

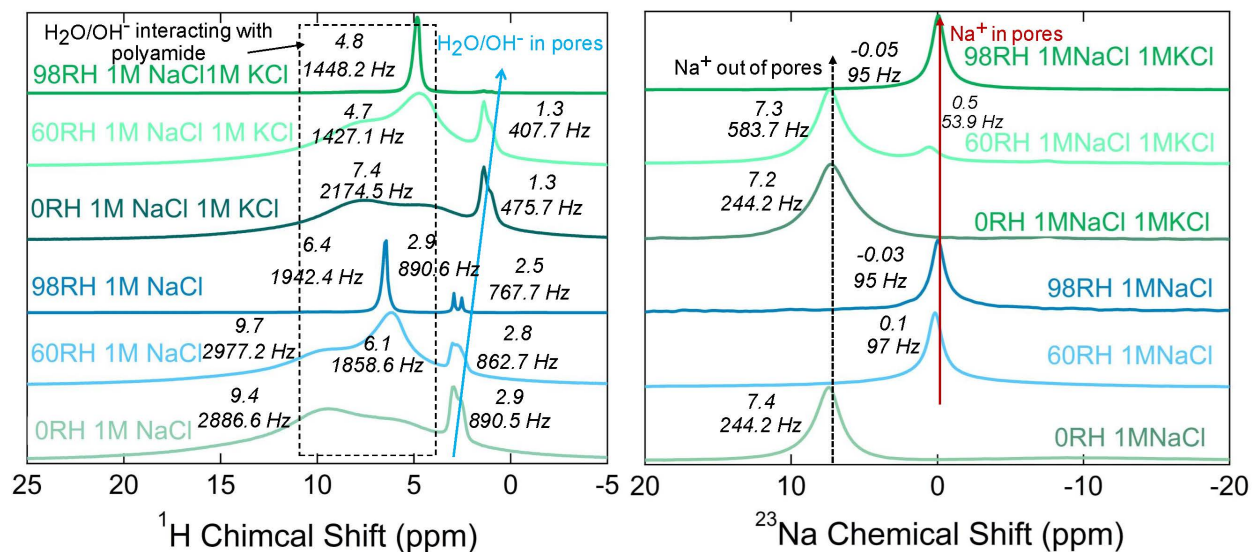


Figure 3: a) ^1H and b) ^{23}Na MAS NMR spectra of ion-exchanged polyamide at different levels of humidity and ionic mixtures. MAS rate: 10 kHz.

The peak positions (chemical changes) of the sodium signal and the line width of ^{23}Na also vary with changes in relative humidity and salinity (Figure 3 b). Without hydration, the (Na^+) movement is attributed to hindered movements outside the pores (Figure 3 -b). At low relative humidity, when salinity increases, the ^{23}Na shift or line-width does not change significantly.

At high relative humidity ($\text{RH} \sim 98\%$), the sodium motion is largely due to polymer-water interactions. With hydration, we observed a sharp peak in the ^1Na spectra, and a shift in the peak position from ~ 7.3 to ~ 0 . This shows that sodium ions move toward the pores of polyamide with increasing humidity (Figure 3 -b). As the sodium peak changes to higher values, the sodium ions interact with the carboxylic acid of polyamide on the surface, since the higher chemical changes for the sodium peaks are usually related to the interaction of sodium with an acidic environment (Figure S5). At higher RH, sodium ions become on average more hydrated and the distance between sodium ions increases, thus reducing the asymmetry in the surrounding electronic environment.⁴² This results in a decrease in electric

field gradients (EFGs) in the ^{23}Na nuclei, leading to a reduced quadrupolar broadening.⁴²

Hydrogen and Sodium Ion Rotational Motion Rates in Polyamide

The parameters of the nuclear spin-lattice relaxation rate (T_1) which accounts for the longitudinal relaxation time, depend on the fluctuation of the nuclear spins of the ions. Therefore, measuring nuclear spin-lattice relaxation rates can provide information regarding the interaction of molecules with their chemical environments.⁴³ In an effort to examine the rotational movement of hydrogen and sodium, we performed spin-lattice relaxation experiments.

We observed that spin-lattice relaxation times (T_1) follow a bimodal distribution of ions attributed to the presence of two different nuclear coordination environments (biexponential relaxation - two components). This is consistent with our NMR PFG experiments and further confirms that the two-site model for bound and unbound ions is appropriate for the polyamide-salt mixture. Bounded ions are located in regions of strong confinement, along with regions where unbounded ions coordinate with other hydrated nuclei.

The T_1 relaxation time for the mobile/unbound site is denoted as T_{1-b} whereas the T_1 relaxation time for the sites with low mobility / bound is indicated as T_{1-a} (Figure 4). For rigid cross-linked polymers, most of the ionic molecular motion near room temperature is in the slow motion region, which means that a longer T_1 suggests slower motion, such as $T_{1-a} > T_{1-b}$.³ When we plot the magnetization intensity as a function of the recovery time for sodium and hydrogen ions in polyamide (Figure S7 and Table S1-S2), we observed that the T_1 relaxation for both hydrogen (Figure 4-a) and sodium ions (Figure 4-b) (bounded and unbounded) continued to increase with salinity (all levels of RH), suggesting that the sodium and hydrogen ionic motions are hindered as the feedstream becomes more concentrated.

For the same salt mixture, as the relative humidity of the polyamide membrane increases, the spin-lattice relaxation time for sodium/hydrogen ions (both bounded and unbounded) becomes shorter, meaning that the overall motion of the fluid-lattice surrounding the ions increases (Figure 4 -a, b). It should be noted that the T_1 values for ^{23}Na in polyamide are

still higher compared to the relaxation times of ^{23}Na in a dilute NaCl solution ($T_1= 49.6$ ms, $T_2= 34.0$ ms)^{44, 45} In summary, the results of relaxation rates for rotational motions of ions follow the same trend as those observed in the study of translation motions derived from diffusion coefficients with respect to varying RH and salinity.

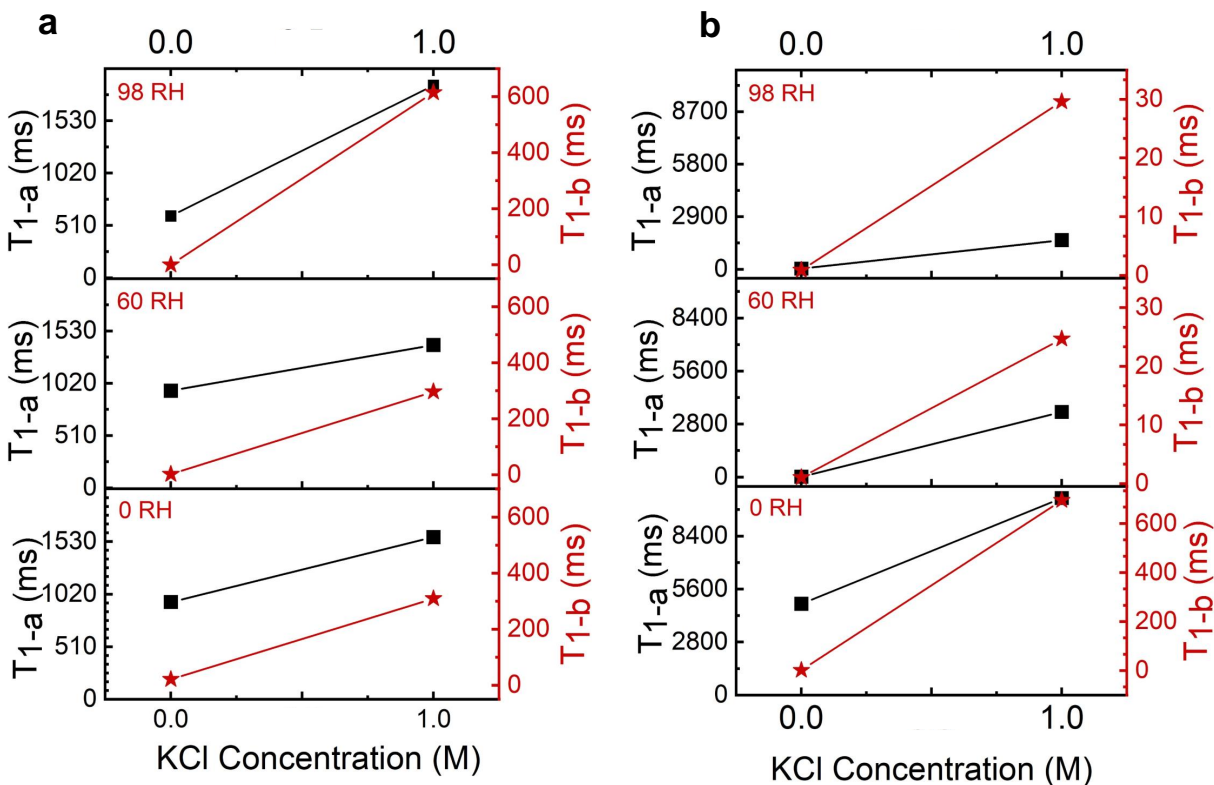


Figure 4: T_1 (component1, left y-axis (Black lines, square symbols)) and T_{1-2} (component 2, right-y axis, red-lines with star symbols) for a) ^1H and b) ^{23}Na NMR of samples with varied concentrations of KCl solution in the ionic mixture. The legend in each graph indicates the relative humidity (RH,%).

Activation Energy for Proton and Sodium Rotational Motions in Polyamide

We have measured the energy barrier (E_a) of proton and sodium ions due to rotational motions by detecting relaxation times as a function of temperature. The T_1 values were measured at four temperatures of 25, 35, 50, and 70 ° C to determine the energy barrier

using Arrhenius plots. In general, ions are able to overcome different hindrances to transport at higher temperatures due to the increased internal energy.¹⁵

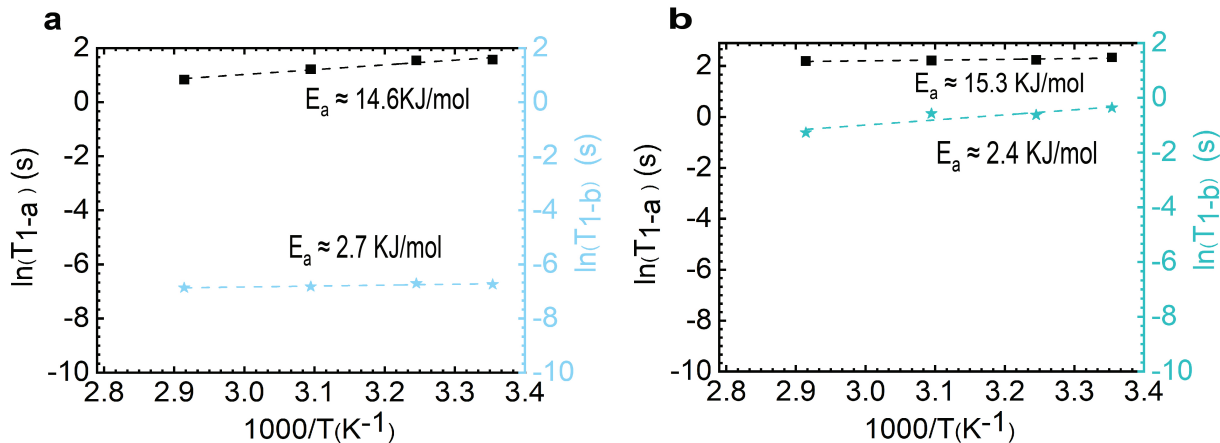


Figure 5: $\ln(T_{1-a})$ (left-axis) and $\ln(T_{1-b})$ (right-axis) of ^{23}Na NMR for ion-exchanged polyamide in a) 1M NaCl, b) 1M NaCl & 1M KCl at the 0 relative humidity (RH, 0%).

We have provided experimental evidence on the rotational energy barrier to elucidate the ion competitive behavior using relaxation experiments at the ≈ 0 relative humidity level. At low relative humidity, we examine the activation of ions in polyamide. Without hydration, the energy barrier is expected to be high because it is the polymer, not the hydrated polymer.

As salinity increases, the activation energy barrier of bounded sodium rotational motions in ion-exchanged polyamide increases from 14.6 KJ/mol (1M NaCl) to 15.3 KJ/mol (1M NaCl & 1M KCl) (Figure 5) while the unbounded sodium ions activation energy barrier did not show a significant dependence on the changes in the ionic mixture. At the molecular level, the bounded sodium remains bounded and the unbounded sodium becomes more bounded with increasing salt amount requiring more energy to overcome the activation energy barrier for motions (Figure S8).

For hydrogen nuclei, we observe that the relationship for rotational relaxation time versus temperature does not necessarily follow a linear trend ($R^2 < 0.9$) (Figure S7, Figure S9). Thereby, we assumed that the dynamics of water in the polyamide at a very low relative humidity level (0 RH) and in the presence of other larger ions (Na, K, Cl) remains bounded.

Therefore, an increase in the temperature of the polyamide environment has not yet overcome the energy barrier for rotational motions without hydration. We hypothesize that the phenomena that water has more affinity to bind to small ions tighter than binding to other water neighboring molecules,⁴⁶ contribute to the bounded water remaining bounded at higher temperatures or KCl amounts. With an increase in the salt in the media, the activation energy barrier for hydrogen rotational motions increases. This increase is due to the increase in hydrogen-frictional interactions with the polyamide material. The frictional effects are due to physical collisions between more potassium ions and rough surfaces, leading to an increased energy barrier.

Ion Dynamics in Polyamide

We illustrate a representative computational model in which the Na^+ and Cl^- ions are distributed with water (Figure 6-a). Our MD simulations were performed using three-dimensional cross-linked PA membrane structures rather than two-dimensional sandwiched PA slab structures⁴⁷ to investigate ion diffusion through the water phase in the PA membrane instead of interfacial ion transport between bulk water and the PA membrane. We carried out all simulations in isothermal-isobaric (NPT) ensemble at 298.15 K and 1 atmospheric pressure conditions until they reached equilibrium states in terms of density and potential energy fluctuations, as indicated in Figure S11 of the supporting information.

The density of the bulk PA structure is determined to be 1.16 g/cm³ and 1.22 g/cm³ at the dry and hydrated states. Systems containing ions are found to have slightly higher density. Table S3 summarizes the average density values obtained from the MD simulations for the three systems. It should be noted that all hydrophilic polar functional groups, such as carboxyl and amino groups, and charged species such as Na^+ and Cl^- are solvated by water molecules in the PA membrane. Therefore, we expect that the dynamics of ions are coupled with that of water molecules. Here, we investigate the self-diffusion (D) of ions and water molecules by analyzing the mean square displacement (MSD) calculated as a function

of time (t) using Equation (1):

$$D = \frac{1}{6} \lim_{t \rightarrow \infty} \frac{1}{t} [(r(t) - r(0))^2] \quad (1)$$

where $r(0)$ and $r(t)$ denote the position of the particle at the beginning and at time t , respectively, and $[(r(t) - r(0))^2]$ is the mean square displacement (MSD).

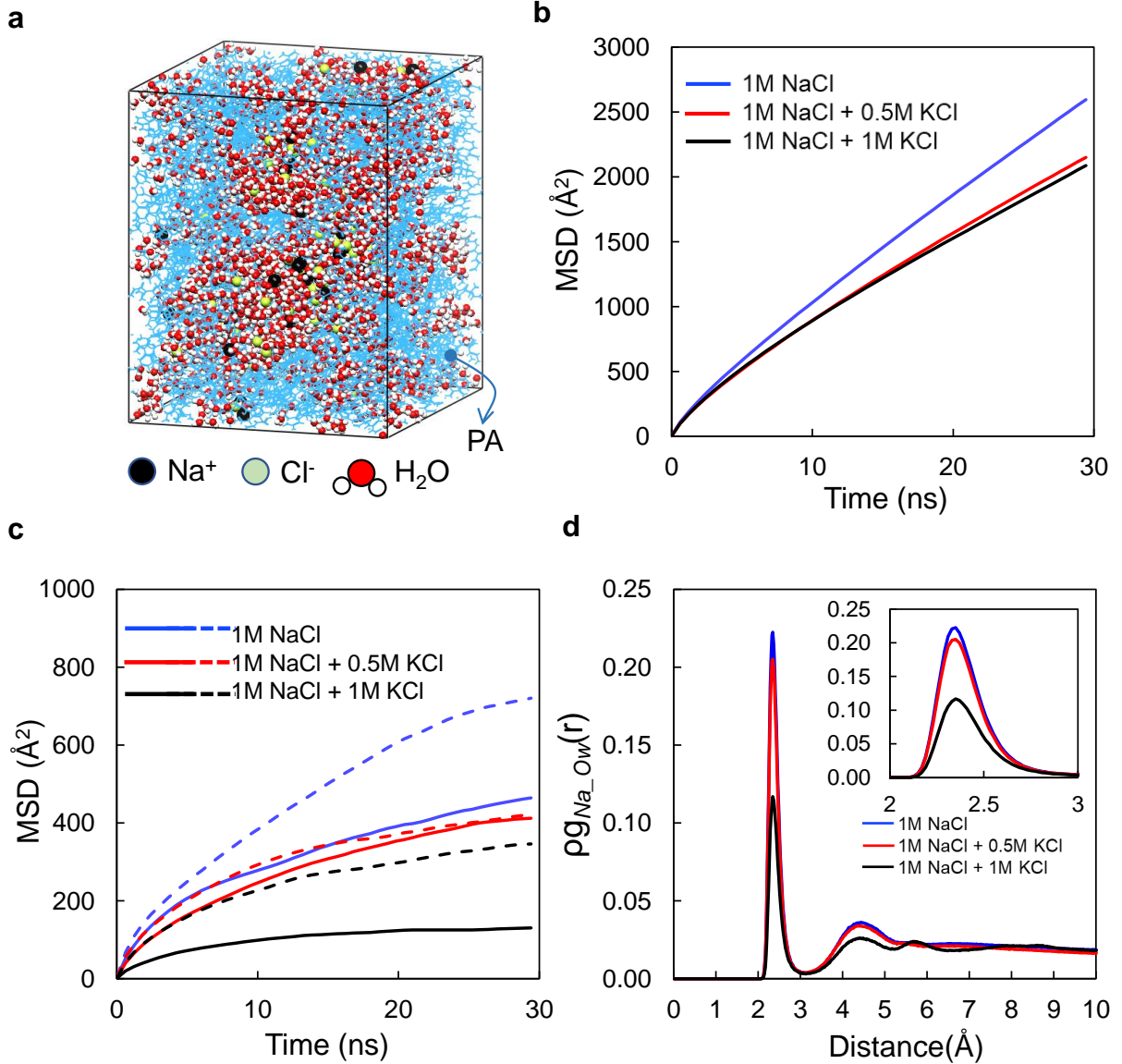


Figure 6: (a) Representative model for cross-linked polyamine membrane with ions solvated in water. The mean square displacement is computed for (b) H₂O and (c) Na⁺ and Cl⁻ ions, where the diffusion of Cl⁻ ion is higher than that of Na⁺. (d) Pair correlation analysis for the Na⁺-O_w of water pair in which the oxygen of H₂O is denoted by O_w

We have demonstrated that (Figures 6 (b) and (c), MSD plots for water) for Na^+ and Cl^- the MSD decreases as the concentration of KCl increases to 1M, and the slope of the linear segment taken from each MSD curve is found to decrease accordingly. These results indicate that the diffusivities of water and ions are reduced with increasing KCl concentration, as summarized in Table S3. The diffusivity of Cl^- is found to be higher than that of Na^+ , which is attributed to the more electrostrict character of water molecules adjacent to the cation compared to anion of the same charge.⁴⁸ Overall, the water diffusion is on the order of magnitude higher than that of ions because the ions in weakly solvated state tend to be associated with surrounding chemical species of PA such as functional groups or neighboring ions via clustering or aggregation for further stabilization, which diminishes the mobility of ions. Therefore, lower diffusion coefficients are expected, especially for the Na^+ ion.

In this paper, we implement pair-correlation analysis between the Na^+ ions and solvating water molecules. We show that the correlation of Na^+ with water molecules decreases as the KCl concentration increases (Figure 6-d). Thus, it is evident that the presence of KCl weakens the solvation state of the Na^+ ion and thereby decreases the Na^+ diffusivity, which emphasizes the sensitivity of the ion mobility in the PA membrane to the local solvation environment.

Conclusion

Here, we used solid-state nuclear magnetic resonance spectroscopy (NMR) to examine the transport of water and salt in polyamide. We investigate the dynamics of H^+ and Na^+ ions at different levels of relative humidity in various salinity environments. We identified "bound" and "unbound" states of water and sodium. These species are attributed to highly immobile, "bound" (or aggregated) sodium/hydrogen, and a significantly more mobile sodium/hydrogen, "unbound", for which the concentration is temperature-, ionic-, and polymer-dependent. The NMR spin-lattice relaxation T_1 shows a behavior consistent with

the transition to a region of rapid hydrogen and sodium motion as T_1 decreases with temperature, concluding that the spin-lattice relaxation obeys the Arrhenius relation where the activation energy barrier of mostly unbounded sodium ions is affected compared to bounded ions. Bounded hydrogen ions remain bounded as the concentration of a competing ion increases (here potassium) or the temperature increases. Therefore, hydrogen ions do not follow the Arrhenius relation or vary in translational/rotational mobility.

Acknowledgments

The authors acknowledge the Office of Naval Research (N00014-20-12559). Y.-Y. Hu and Y. Chen acknowledge the support from National Science Foundation under Grant no. DMR-1847038

Materials and Methods

Materials

The following materials have been purchased from Sigma-Aldrich and have been used as received without further purification: Trimesoyl chloride (TMC) 98%, m-phenylenediamine (MPD) flakes > 99%, anhydrous sodium chloride (NaCl, >99%), anhydrous potassium chloride (KCl, >99%), Phosphorus pentoxide, potassium sulphate, and magnesium nitrate. Methanol, ethanol, and n-hexane were purchased from VWR International Ltd. Deionized (DI) water (18.2 Ω) was prepared in a millipore Milli-Q purification system.

Polyamide Membrane Preparation

Polyamide membranes for NMR experiments were synthesized via interfacial polymerization method by adding 0.1 % (w/v) trimesoyl chloride (TMC, Sigma-Aldrich) in n-hexane solution into 2 % (w/v) aqueous m-phenylenediamine (MPD, Sigma-Aldrich) solution. Free-

standing interfacial polymerization has been a well-known technique to form the selective top layer of reverse osmosis membranes for advanced characterization purposes where the polyamide layer has been synthesized without the need for a ultrafiltration support membrane⁴⁹. The polyamide film would form at the water-oil solution interface instantaneously by a self-limiting reaction. In the interfacial polymerization method, the polyamide layer is formed by diffusion of MPD molecules toward the oil-water interface and reaction with TMC acid chloride groups. It has been hypothesized that nanofilms form by nucleation and aggregation of different molecular weight of oligomers at the interface and the form a continuous film under prolonged reaction time.⁴⁹ The interfacial reaction proceeded without stirring, and the fragments of the polymer film formed at the solution interface were retrieved and precipitated in deionized water. The formed polyamide films were dried at 90 C for 4 minutes, and neutralized with 0.2 wt.% sodium carbonate solution and then washed generously with deionized water and methanol to remove unreacted monomer and formed salt. The synthesized polyamide membranes were ion-exchanged for further experiments. For ion-exchanging the polyamide membranes materials, the synthesized polyamide was immersed in solutions of 1 M NaCl, 1 M NaCl + 0.5 M KCl, and 1 M NaCl + 1 M KCl stirring for 24 hours using magnetic stirrer. Afterwards, the polyamide was retrieved from the solutions using vacuum filtration. Dried ion-exchanged polyamide membranes containing different ionic mixtures (ionic strength of 1M and 2M) were partially rehydrated by exposure to different levels of relative humidity (0, 60 and 98%). The samples were then stored in desiccators where we controlled the environment of the desiccator for relative humidity levels using saturated solutions of organic salts for at least 48 hours prior to NMR experiment. We probed the relative humidity of the environments using a high-precision hygrometer/thermometer (Cole-Parmer). To obtain relative humidity levels of 0, 60, and 98 RH, we used inorganic salts of phosphorous pentoxide, magnesium nitrate, and potassium sulphate respectively. We characterized the pure polyamide using solid-state ¹ H and ¹³ C NMR spectra upon synthesis before introducing ionic salt solutions in the sample (Figure S11-S12).

Polyamide Water Uptake, Density, and Elemental composition Measurements

The water uptake were measured by comparing the wet and dry state of polyamide membranes at room temperature. The water uptake was calculated using following equation:

$$\text{Water Uptake} = \left(\frac{W_w - W_d}{W_d} \right) \times 100(\%) \quad (2)$$

Where W_w and W_d are the masses of fully hydrated and dry polyamide samples, respectively. We measured the mass of fully hydrated polyamide samples after we wiped off the excess surface water with tissue paper. In this work, the polyamide water uptake is measured to be 29.1 %. Additionally, we determined the density of polyamide with use of DI water at room temperature using density measurement kit (VWR International) via an analytical balance and the synthesized polyamide density was measured to be 1.35 g/cm³. The surface chemistry of synthesized polyamide were investigated with X-ray photoelectron spectroscopy (XPS) revealing atomic elemental composition for synthesized polyamide be 67.6 % C (carbon), 28.9 % O (oxygen), and 3.5 % N (nitrogen).

NMR Characterization

All the NMR data for polyamide characterizations were obtained using the NMR research facilities at Georgia Institute of Technology. The solid-state NMR characterization was performed on a Bruker AV3 HD 300 NMR spectrometer (Bruker, Rheinstetten, Germany) operating at an MAS frequency of 10 kHz for ²³Na and ¹H. Polymers were tightly packed into 4 mm Bruker MAS rotors which were then exposed to various relative humidity levels by placing the rotor over different inorganic salt solutions in sealed environments. Before measurement, the rotor was removed from the sealed environment and quickly capped. MAS NMR experiments were performed at 10-kHz spinning speeds. NMR spectra under static conditions were also recorded. Spin-lattice relaxation times (T_1) were measured using a

standard saturation recovery sequence. The diffusion coefficient, relaxation, and activation energy barriers have been provided in the result and discussion section.

Diffusion Measurement

Diffusion measurements were carried out using a pulsed field gradient (PFG) method at 25 °C on a Bruker AV III 400 spectrometer. In a PFG experiment, with applying external magnetic field, spins of nuclei are being decoded position-wise called spatial labelling which can be observed by a period of observation time allowing diffusion of ions happen. This will cause dephasing in magnetization and decrease in signal intensity.⁴⁵ We determined the diffusion coefficients from the exponential decay of peak intensities over a range of applied gradients.⁴⁵ The Stejskal-Tanner equation describes the signal attenuation that results from diffusion in the PFG experiment. 16 to 32 gradient steps were applied and the number of scans varied from 4 to 64 to yield sufficient signal-to-noise ratio. Diffusion was measured along the magnetic field (z) direction. Acquisitions for a series of b-value were obtained by stepping the strength of the gradient, where b is defined as seen in the Stejskal-Tanner equation below.⁵⁰

$$I = I_0 e^{-D\gamma^2 g^2 \delta^2 (\Delta - \delta/3)} = I_0 e^{-bD} \quad (3)$$

where I is intensity/integral of the peak at a given g, I_0 is intensity/integral of the peak at $G=0$, γ is the gyromagnetic ratio of the nucleus (for ^1H , $\gamma = 267.522 \times 10^6$ rad/s.T, and for ^{23}Na , $\gamma = 70.761 \times 10^6$ rad/s.T), δ is the effective applied gradient pulse width (1 ms), Δ is the time duration of the applied gradient (50 ms), G is the field strength (maximum gradient strengths ranged from 0-200 G/cm for ^1H and 0-800 G/cm for ^{23}Na), and D is the diffusion coefficient. The diffusion coefficients, D, was obtained by fitting the I/I_0 data, obtained from a PFG experiment, as a function of g.⁵¹

NMR Data Analysis

The NMR data were processed using the TopSpin software (Bruker, Rheinstetten, Germany). The fitting equation used to analyzing T_1 spin-lattice relaxation times is described below. The saturation recovery is characterized by an exponential function:⁵²

$$M(\tau) = M_0(1 - \exp(\frac{t}{\tau})) \quad (4)$$

In many instances data could not be fitted with the single exponential recovery of the above equation. Good fits were obtained with a two-component model according to following equation:

$$M(\tau) = M(0) + M(0)'(1 - \exp(\frac{-t}{T_{1-a}}) + M(0)''(1 - \exp(\frac{-t}{T_{1-b}})) \quad (5)$$

For activation energy measurements, where the relaxation time is temperature dependent, we used the following equation to calculate the activation energy:

$$\frac{1}{T_1} = A \exp(\frac{-E_a}{RT}) \quad (6)$$

where E_a is the activation energy, R is ideal gas constant, T is the temperature in Kelvin, and A is the pre-exponential factor.⁵³

Computational Details

We investigated the ion diffusion in hydrated polyamide (PA) structures using molecular dynamics (MD) simulation method. To model a cross-linked PA membrane via simulations, first, we mixed trimesoyl chloride (TMC) and M-phenylenediamine (MPD) in 1:2 molar ratio and performed MD simulation to prepare equilibrated structure, and then made the bonds between amine and carboxyl groups which were located closely in order to obtain a cross-linked PA structure. Once the bulk structure was fabricated, it was hydrated by adding water

content of 29.1 wt% which was determined in experiments. Next, Na⁺, K⁺, and Cl⁻ ions were introduced into the system with predetermined conditions: i) 1 M NaCl, ii) 1 M NaCl 0.5 M KCl, and iii) 1 M NaCl + 1 M KCl. In our MD simulations, we employed the F3C forcefield⁵⁴ to describe water molecules, and a set of Lennard-Jones parameters developed by Yagasaki et al.⁵⁵ for Na⁺, K⁺, and Cl⁻ ions, which has been reported to successfully reproduce the solubility of ions avoiding spontaneous ion aggregation in the vicinity of biomolecules.^{56,57} For all other pairwise interatomic interaction parameters, we employed the DREIDING forcefield.⁵⁸ Atomic charges for the description of Coulombic interactions were determined by Mulliken population analysis computed by a Jaguar⁵⁹ with the B3LYP functional and 6-31G** basis set, where DFT-D3⁶⁰ correction was used for van der Waals interaction between atoms. MD simulations were performed using the LAMMPS⁶¹ software package.

References

- (1) Geise, G. M.; Park, H. B.; Sagle, A. C.; Freeman, B. D.; McGrath, J. E. Water permeability and water/salt selectivity tradeoff in polymers for desalination. *Journal of Membrane Science* **2011**, *369*, 130–138.
- (2) Epsztein, R.; DuChanois, R. M.; Ritt, C. L.; Noy, A.; Elimelech, M. Towards single-species selectivity of membranes with subnanometre pores. *Nat. Nanotechnol.* **2020**, *15*, 426–436.
- (3) Kwak, S.-Y.; Woo Ihm, D. Use of atomic force microscopy and solid-state NMR spectroscopy to characterize structure-property-performance correlation in high-flux reverse osmosis (RO) membranes. *Journal of Membrane Science* **1999**, *158*, 143–153.
- (4) Abbaszadeh, M.; Krizak, D.; Kundu, S. Layer-by-layer assembly of graphene oxide nanoplatelets embedded desalination membranes with improved chlorine resistance. *Desalination* **2019**, *470*, 114116.

- (5) Wang, L.; Cao, T.; Dykstra, J. E.; Porada, S.; Biesheuvel, P. M.; Elimelech, M. Salt and Water Transport in Reverse Osmosis Membranes: Beyond the Solution-Diffusion Model. *Environmental Science & Technology* **2021**, *55*, 16665–16675, Publisher: American Chemical Society.
- (6) Ritt, C. L.; Stassin, T.; Davenport, D. M.; DuChanois, R. M.; Nulens, I.; Yang, Z.; Benzvi, A.; Segev-Mark, N.; Elimelech, M.; Tang, C. Y.; Ramon, G. Z.; Vankelecom, I. F. J.; Verbeke, R. The open membrane database: Synthesis–structure–performance relationships of reverse osmosis membranes. *Journal of Membrane Science* **2022**, *641*, 119927.
- (7) Li, D.; Wang, H. Recent developments in reverse osmosis desalination membranes. **2010**, *20*, 4551–4566, Publisher: Royal Society of Chemistry.
- (8) Paul, D. R. The Solution-Diffusion Model for Swollen Membranes. *Separation and Purification Methods* **1976**, *5*, 33–50.
- (9) Wijmans, J. G.; Baker, R. W. The solution-diffusion model: a review. *Journal of Membrane Science* **1995**, *107*, 1–21.
- (10) Verliefde, A. R. D.; Van der Meeren, P.; Van der Bruggen, B. *Encyclopedia of Membrane Science and Technology*; John Wiley & Sons, Ltd, 2013; pp 1–26.
- (11) Biesheuvel, P. M.; Zhang, L.; Gasquet, P.; Blankert, B.; Elimelech, M.; van der Meer, W. G. J. Ion Selectivity in Brackish Water Desalination by Reverse Osmosis: Theory, Measurements, and Implications. *Environ. Sci. Technol. Lett.* **2020**, *7*, 42–47, Publisher: American Chemical Society.
- (12) Wang, R.; Lin, S. Pore model for nanofiltration: History, theoretical framework, key predictions, limitations, and prospects. *Journal of Membrane Science* **2021**, *620*, 118809.

- (13) Hegde, V. H.; Doherty, M. F.; Squires, T. M. A two-phase model that unifies and extends the classical models of membrane transport. *Science* **2022**, *377*, 186–191, Publisher: American Association for the Advancement of Science.
- (14) Shaffer, D. L.; Arias Chavez, L. H.; Ben-Sasson, M.; Romero-Vargas Castrillón, S.; Yip, N. Y.; Elimelech, M. Desalination and Reuse of High-Salinity Shale Gas Produced Water: Drivers, Technologies, and Future Directions. *Environ. Sci. Technol.* **2013**, *47*, 9569–9583, Publisher: American Chemical Society.
- (15) Shefer, I.; Peer-Haim, O.; Leifman, O.; Epsztein, R. Enthalpic and Entropic Selectivity of Water and Small Ions in Polyamide Membranes. *Environ. Sci. Technol.* **2021**, *55*, 14863–14875, Publisher: American Chemical Society.
- (16) Reif, B.; Ashbrook, S. E.; Emsley, L.; Hong, M. Solid-state NMR spectroscopy. *Nat Rev Methods Primers* **2021**, *1*, 1–23.
- (17) Bone, S. E.; Steinrück, H.-G.; Toney, M. F. Advanced Characterization in Clean Water Technologies. *Joule* **2020**, *4*, 1637–1659.
- (18) Culp, T. E.; Khara, B.; Brickey, K. P.; Geitner, M.; Zimudzi, T. J.; Wilbur, J. D.; Jons, S. D.; Roy, A.; Paul, M.; Ganapathysubramanian, B.; Zydney, A. L.; Kumar, M.; Gomez, E. D. Nanoscale control of internal inhomogeneity enhances water transport in desalination membranes. *Science* **2021**, *371*, 72–75.
- (19) G. Pate, S.; Xu, H.; P. O'Brien, C. Operando observation of CO₂ transport intermediates in polyvinylamine facilitated transport membranes, and the role of water in the formation of intermediates, using transmission FTIR spectroscopy. *Journal of Materials Chemistry A* **2022**, *10*, 4418–4427.
- (20) Hatzell, M. C.; Turhan, A.; Kim, S.; Hussey, D. S.; Jacobson, D. L.; Mench, M. M. Quantification of Temperature Driven Flow in a Polymer Electrolyte Fuel Cell Using

- High-Resolution Neutron Radiography. *J. Electrochem. Soc.* **2011**, *158*, B717, Publisher: IOP Publishing.
- (21) Foglia, F.; Frick, B.; Nania, M.; Livingston, A. G.; Cabral, J. T. Multimodal confined water dynamics in reverse osmosis polyamide membranes. *Nature communications* **2022**, *13*, 1–11.
- (22) Sharma, V. K.; Singh, P. S.; Gautam, S.; Maheshwari, P.; Dutta, D.; Mukhopadhyay, R. Dynamics of water sorbed in reverse osmosis polyamide membrane. *Journal of Membrane Science* **2009**, *326*, 667–671.
- (23) Zhang, N.; Chen, S.; Yang, B.; Huo, J.; Zhang, X.; Bao, J.; Ruan, X.; He, G. Effect of Hydrogen-Bonding Interaction on the Arrangement and Dynamics of Water Confined in a Polyamide Membrane: A Molecular Dynamics Simulation. *J. Phys. Chem. B* **2018**, *122*, 4719–4728, Publisher: American Chemical Society.
- (24) Chen, G. Q.; Scholes, C. A.; Doherty, C. M.; Hill, A. J.; Qiao, G. G.; Kentish, S. E. Modeling of the sorption and transport properties of water vapor in polyimide membranes. *Journal of Membrane Science* **2012**, *409-410*, 96–104.
- (25) Xu, X.; Kirkpatrick, R. J. NaCl interaction with interfacially polymerized polyamide films of reverse osmosis membranes: A solid-state ^{23}Na NMR study. *Journal of Membrane Science* **2006**, *280*, 226–233.
- (26) Nieuwendaal, R. C.; Wilbur, J. D.; Welsh, D.; Witherspoon, V.; Stafford, C. M. A method to quantify composition, purity, and cross-link density of the active polyamide layer in reverse osmosis composite membranes using ^{13}C cross polarization magic angle spinning nuclear magnetic resonance spectroscopy. *Journal of Membrane Science* **2022**, *648*, 120346.
- (27) Kwak, S.-Y. Relationship of relaxation property to reverse osmosis permeability in aromatic polyamide thin-film-composite membranes. *Polymer* **1999**, *40*, 6361–6368.

- (28) Artemov, D. Y.; Samoilenko, A. A.; Iordanskii, A. L. Study of diffusion of water in polyamide-6 using nuclear magnetic resonance intrascopy. *Polymer Science U.S.S.R.* **1989**, *31*, 2709–2713.
- (29) Slichter, W. P. Proton Magnetic Resonance in Polyamides. *Journal of Applied Physics* **1955**, *26*, 1099–1103, Publisher: American Institute of Physics.
- (30) Puffr, R.; Šebenda, J. On the Structure and Properties of Polyamides. XXVII. The Mechanism of Water Sorption in Polyamides. *Journal of Polymer Science Part C: Polymer Symposia* **1967**, *16*, 79–93.
- (31) Turoscy, R.; Leidheiser, H.; Roberts, J. E. Solid-State Nuclear Magnetic Resonance Studies of Ions in Protective Coatings III : Sodium, Lithium, and Cesium Ions in Polyimide and Epoxy-Polyamide Coatings. *J. Electrochem. Soc.* **1993**, *140*, 149, Publisher: IOP Publishing.
- (32) Callaghan, P. T. *Translational Dynamics and Magnetic Resonance: Principles of Pulsed Gradient Spin Echo NMR*; Oxford University Press, 2011; p 576.
- (33) Arges, C. G.; Ramani, V. Two-dimensional NMR spectroscopy reveals cation-triggered backbone degradation in polysulfone-based anion exchange membranes. *Proceedings of the National Academy of Sciences* **2013**, *110*, 2490–2495.
- (34) Sharma, V. K.; Singh, P. S.; Gautam, S.; Mitra, S.; Mukhopadhyay, R. Diffusion of water in nanoporous NF polyamide membrane. *Chemical Physics Letters* **2009**, *478*, 56–60.
- (35) Muscatello, J.; Müller, E. A.; Mostofi, A. A.; Sutton, A. P. Multiscale molecular simulations of the formation and structure of polyamide membranes created by interfacial polymerization. *Journal of Membrane Science* **2017**, *527*, 180–190.

- (36) Anderson, J. L.; Quinn, J. A. Restricted Transport in Small Pores: A Model for Steric Exclusion and Hindered Particle Motion. *Biophysical Journal* **1974**, *14*, 130–150.
- (37) Bouazizi, S.; Nasr, S. Self-diffusion coefficients and orientational correlation times in aqueous NaCl solutions: Complementarity with structural investigations. *Journal of Molecular Liquids* **2011**, *162*, 78–83.
- (38) Peeters, J. M. M.; Boom, J. P.; Mulder, M. H. V.; Strathmann, H. Retention measurements of nanofiltration membranes with electrolyte solutions. *Journal of Membrane Science* **1998**, *145*, 199–209.
- (39) Tan, R. et al. Hydrophilic microporous membranes for selective ion separation and flow-battery energy storage. *Nature Materials* **2020**, *19*, 195–202.
- (40) Abragam, A. *The Principles of Nuclear Magnetism*; 1961.
- (41) Cahill, D. G.; Freger, V.; Kwak, S.-Y. Microscopy and Microanalysis of Reverse-Osmosis and Nanofiltration Membranes. *MRS Bulletin* **2008**, *33*, 27–32, Publisher: Cambridge University Press.
- (42) Chen, Y.; Lingwood, M. D.; Goswami, M.; Kidd, B. E.; Hernandez, J. J.; Rosenthal, M.; Ivanov, D. A.; Perlich, J.; Zhang, H.; Zhu, X.; Möller, M.; Madsen, L. A. Humidity-Modulated Phase Control and Nanoscopic Transport in Supramolecular Assemblies. *J. Phys. Chem. B* **2014**, *118*, 3207–3217.
- (43) Yan, L.; Hu, Y.; Zhang, X.; Yue, B. In *Annual Reports on NMR Spectroscopy*; Webb, G. A., Ed.; Academic press, 2016; Vol. 88; pp 149–213.
- (44) Guo, X.; Theissen, S.; Claussen, J.; Hildebrand, V.; Kamphus, J.; Wilhelm, M.; Luy, B.; Guthausen, G. Dynamics of Sodium Ions and Water in Swollen Superabsorbent Hydrogels as Studied by ^{23}Na - and ^1H -NMR. *Macromolecular Chemistry and Physics* **2019**, *220*, 1800350.

- (45) Engelke, S.; E. Marbella, L.; M. Trease, N.; Volder, M. D.; P. Grey, C. Three-dimensional pulsed field gradient NMR measurements of self-diffusion in anisotropic materials for energy storage applications. *Physical Chemistry Chemical Physics* **2019**, *21*, 4538–4546.
- (46) Hribar, B.; Southall, N. T.; Vlachy, V.; Dill, K. A. How Ions Affect the Structure of Water. *J. Am. Chem. Soc.* **2002**, *124*, 12302–12311.
- (47) Ding, M.; Szymczyk, A.; Ghoufi, A. Hydration of a polyamide reverse-osmosis membrane. *Journal of Membrane Science* **2016**, *501*, 248–253.
- (48) Vitagliano, V.; Lyons, P. A. Diffusion coefficients for aqueous solutions of sodium chloride and barium chloride. *Journal of the American Chemical Society* **1956**, *78*, 1549–1552.
- (49) Karan, S.; Jiang, Z.; Livingston, A. G. Sub–10 nm polyamide nanofilms with ultrafast solvent transport for molecular separation. *Science* **2015**, *348*, 1347–1351.
- (50) Stejskal, E. O.; Tanner, J. E. Spin Diffusion Measurements: Spin Echoes in the Presence of a Time-Dependent Field Gradient. *J. Chem. Phys.* **1965-01**, *42*, 288–292.
- (51) Chang, K.; Korovich, A.; Xue, T.; Morris, W. A.; Madsen, L. A.; Geise, G. M. Influence of Rubbery versus Glassy Backbone Dynamics on Multiscale Transport in Polymer Membranes. *Macromolecules* **2018**, *51*, 9222–9233, American Chemical Society.
- (52) Keeler, J. *Understanding NMR Spectroscopy*; John Wiley & Sons, 2011.
- (53) Foster, R. J.; Damion, R. A.; Ries, M. E.; Smye, S. W.; McGonagle, D. G.; Binks, D. A.; Radjenovic, A. Imaging of nuclear magnetic resonance spin–lattice relaxation activation energy in cartilage. *Royal Society Open Science* **2018**, *5*, 180221.
- (54) Levitt, M.; Hirshberg, M.; Sharon, R.; Laidig, K. E.; Daggett, V. Calibration and

- Testing of a Water Model for Simulation of the Molecular Dynamics of Proteins and Nucleic Acids in Solution. *J. Phys. Chem. B* **1997**, *101*, 5051–5061.
- (55) Yagasaki, T.; Matsumoto, M.; Tanaka, H. Lennard-Jones Parameters Determined to Reproduce the Solubility of NaCl and KCl in SPC/E, TIP3P, and TIP4P/2005 Water. *J. Chem. Theory Comput.* **2020**, *16*, 2460–2473, Publisher: American Chemical Society.
- (56) Auffinger, P.; Cheatham, T. E.; Vaiana, A. C. Spontaneous Formation of KCl Aggregates in Biomolecular Simulations: A Force Field Issue? *J. Chem. Theory Comput.* **2007**, *3*, 1851–1859, Publisher: American Chemical Society.
- (57) Savelyev, A.; Papoian, G. A. Electrostatic, Steric, and Hydration Interactions Favor Na⁺ Condensation around DNA Compared with K⁺. *J. Am. Chem. Soc.* **2006**, *128*, 14506–14518.
- (58) Mayo, S. L.; Olafson, B. D.; Goddard, W. A. DREIDING: a generic force field for molecular simulations. *Journal of Physical chemistry* **1990**, *94*, 8897–8909.
- (59) Bochevarov, A. D.; Harder, E.; Hughes, T. F.; Greenwood, J. R.; Braden, D. A.; Philipp, D. M.; Rinaldo, D.; Halls, M. D.; Zhang, J.; Friesner, R. A. Jaguar: A high-performance quantum chemistry software program with strengths in life and materials sciences. *International Journal of Quantum Chemistry* **2013**, *113*, 2110–2142.
- (60) Grimme, S.; Antony, J.; Ehrlich, S.; Krieg, H. A consistent and accurate ab initio parametrization of density functional dispersion correction (DFT-D) for the 94 elements H-Pu. *The Journal of chemical physics* **2010**, *132*, 154104.
- (61) Plimpton, S. Fast parallel algorithms for short-range molecular dynamics. *Journal of computational physics* **1995**, *117*, 1–19.